Adhesion and Friction Mechanisms of Polymer-on-Polymer Surfaces

Nobuo Maeda, Nianhuan Chen, Matthew Tirrell, Jacob N. Israelachvili*

The adhesion and friction of smooth polymer surfaces were studied below the glass transition temperature by use of a surface forces apparatus. The friction force of a crosslinked polymer was orders of magnitude less than that of an uncrosslinked polymer. In contrast, after chain scission of the outermost layers, the adhesion hysteresis and friction forces increase substantially. These results show that polymer-polymer adhesion hysteresis and friction depend on the dynamic rearrangement of the outermost polymer segments at shearing interfaces, and that both increase as a transition is made from crosslinked surfaces to surfaces with long chains to surfaces with quasi-free ends. The results suggest new ways for manipulating the adhesion and friction of polymer surfaces by adjusting the state of the surface chains.

Polymers are often used as adhesive and lubricant coatings to produce both high and low adhesion or friction. Characterization of tribological and adhesive properties and dynamics has been of great interest for many years. Most tribological studies have, however, been limited to macroscopic or microscopic systems, because of a lack of experimental nanoscale techniques and the molecular-level complexity of these systems. With the miniaturization of machinery and computer-related devices, there is now a practical need to understand these phenomena at the molecular level.

There is a close correlation between adhesion hysteresis, where the work needed to separate two surfaces or molecules is generally greater than that originally gained on bringing them together, and friction forces. Such correlations have been experimentally demonstrated in studies of the adhesion and friction of adsorbed surfactant layers with each other (symmetric system) (*1*) and of polymer surfaces with mica (asymmetric system) (*2, 3*). These correlations can be understood from simple thermodynamic considerations (*4*), as well as more sophisticated theories and simulations (*5*). For surfaces composed of chain molecules, their adhesion hysteresis is largely determined by the rearrangement or restructuring of surface molecular groups to enhance the number and/or strength of contacting bonds (e.g., interdigitating chain segments) across the interface (*6*). Earlier work with surfactant-coated surfaces containing short hydrocarbon chains indicated that the state of the outermost molecular groups plays a crucial role in determining the extent and dynamics of these processes, and that even a small amount of interdigitation can significantly enhance their adhesion hysteresis and friction (*1*). This is illustrated in Fig. 1A, which shows how only one or two methylene groups, each of segment length 1.25 Å, need to interdigitate with or penetrate into the opposite surface to increase the number of van der Waals bonds by an order of magnitude, in addition to presenting a much larger steric barrier or angle shear. As we shall see, this example for short [low molecular weight (MW)] hydrocarbon chains is important for understanding the adhesion hysteresis and friction of high MW polymer surfaces. This phenomenon is already exploited to strengthen the interfacial adhesion between two immiscible polymers through the addition of a mutually miscible diblock copolymer (*7*). However, data on the adhesion and cohesion of polymer surfaces have yet to be related to their friction.

Polystyrene (PS) is a nonpolar polymer which is glassy at room temperature. Polyvinyl benzyl chloride (PVBC) is structurally similar to PS, except that one of the hydrogen atoms in the benzene ring is replaced by $-CH_2Cl$, thus inducing polarity in each segment (Fig. 1). These two polymers are ideal for the purpose of examining the effect of polarity on friction and adhesion, and recent measurements of adhesion hysteresis between polymers of different polarity found that polymers of larger polarity tend to have larger adhesion hysteresis (*8*). Both PS ($M_w \approx 100,000$) and PVBC ($M_w \approx 25,000$) were purchased from Sigma-Aldrich and used without further purification. Each polymer film was prepared by dipping a mica substrate

---

Department of Chemical Engineering, Materials Department, and Materials Research Laboratory, College of Engineering, University of California, Santa Barbara, CA 93106, USA.

*To whom correspondence should be addressed. E-mail: jacob@engineering.ucsb.edu

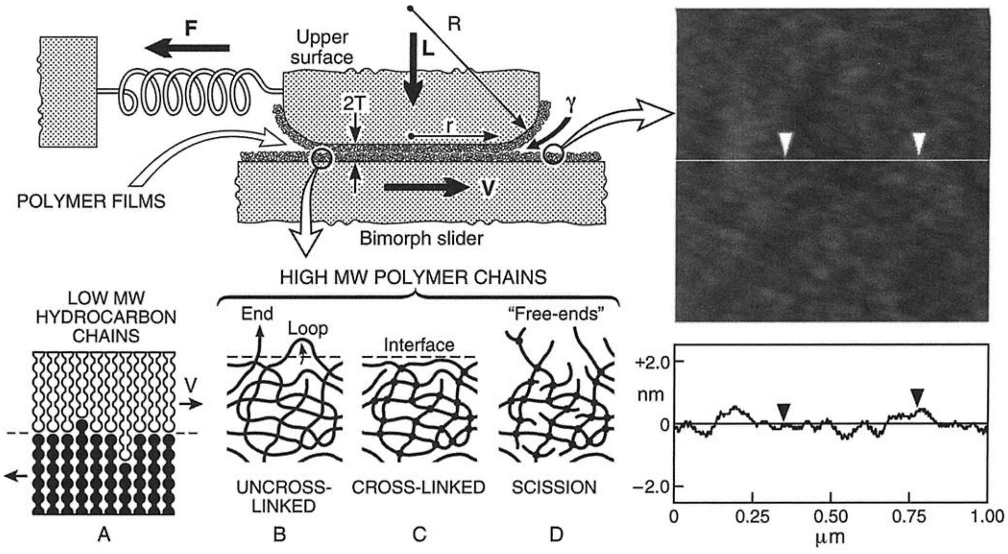

Fig. 1. Experimental geometry in the surface forces apparatus (SFA). The polymer films of thickness *T* are supported by 2- to 3-μm-thick freshly cleaved mica sheets. The undeformed radii of curvature of the surfaces *R* are typically 2 cm and the (adhesive) contact diameter 2*r* at zero external load *L* is typically 60 μm. Friction forces *F* at different sliding velocities *V* and applied loads *L* were measured in these experiments. Atomic force micrograph of a typical PS surface prepared by the dipping method is shown on the right; the root-mean-square surface roughness is about 0.5 nm. (**A**) Schematic of interdigitating short-chained hydrocarbon segments across an adhering or shearing interface. (**B**) Schematic of uncrosslinked high-MW polymer interface (only one surface shown) as the coils of the lower surface slowly interpenetrate into the opposite surface. (**C**) Crosslinked polymer surface. (**D**) Polymer surface after scission, which exposes distally free ends that can rapidly penetrate into the opposite surface.

mounted on a silica disk into a prefiltered (200 nm mesh size) polymer solution in toluene. The thickness *T* of the polymer film was controlled by adjusting the concentration of the toluene solution. Films thus prepared are very smooth (Fig. 1), but the maximum *T* is limited by the wetting properties of the solution on mica and the solubility of the polymer in toluene. Thus, for PS, a ~5 weight percent (wt %) solution resulted in a ~0.19-μm-thick film, and a ~10 wt % solution resulted in a ~1.5-μm-thick film. For the more toluene-soluble PVBC, a ~10 wt % solution resulted in a ~0.16-μm-thick film. The surfaces were then dried in a vacuum oven for >12 hours before mounting into a surface forces apparatus (SFA) (*9*). The range of film thicknesses studied, after drying, varied from $T = 0.08$ to 1.5 μm for PS, and $T = 0.10$ to 0.16 μm for PVBC.

In the SFA, shown schematically in Fig. 1, one of the surfaces is driven at a given amplitude (typically 60 μm) parallel to the other surface at various frequencies, using a piezoelectric bimorph slider controlled by a function generator (HP 3325B, Hewlett-Packard) (*9*). A triangular input signal was used to move the lower surface at a constant speed *V* in both directions. The friction forces *F* were detected by semiconductor strain gauges attached to cantilever springs supporting the second (upper) surface. The applied loads or adhesion forces *L* between the surfaces were measured using a normal spring (typical spring constant: 640 N/m). Contact radii *r*, deformations of the surfaces, and refractive index changes (arising, for example, from the flow and build-up of polymer around the contact zone) were monitored during experiments by observing and recording the optical interference fringes of equal chromatic order (FECO) (*10*). The temperature of the SFA chamber was controlled and monitored to within ±0.1°C. We concentrate on the results obtained at 25°C for both polymers (*11*). In all, several successful experiments, each conducted at a number of separate contact positions, were performed, giving consistent results, both qualitatively and quantitatively.

There are several qualitative features that are common to both uncrosslinked polymers, such as the stick-slip friction profiles (Fig. 2). Each profile describes the friction force as a function of time or sliding distance at constant sliding speed. Decaying stick-slip is observed at slow speeds (Fig. 2A). If the motion continues for a sufficiently long distance in one direction, the decay is complete within one cycle of the sliding motion, and the stick maxima and slip minima merge into a smooth, continuous line that constitutes the constant "steady-state" friction force (Fig. 2A). The steady-state friction appears to be more an extension of the slips rather than the sticks (Fig. 2A). This suggests that the polymer chains that get entangled during sticking gradually disentangle during slipping. The transition from stick-slip to smooth sliding occurs more readily (with fewer stick-slip events) at higher sliding speeds. At sufficiently high speeds, smooth sliding occurs from the onset of sliding, except for a small, single stiction spike (Fig. 2B). With respect to the adhesion hysteresis of these uncrosslinked polymers, both PS and PVBC exhibit only a small and similar adhesion hysteresis at 25°C (Fig. 3, A and C). The friction and adhesion hysteresis of the uncrosslinked polymers may be attributed to the entanglement (interpenetration) and restructuring of their surface segments: initially, the surfaces will have mainly flat coils which will penetrate into the other surface mainly as loops (*12*) but with a few ends, due to the high MW (Fig. 1B).

The in situ crosslinking of polymer films (i.e., films that are already mounted in the SFA chamber) was easily achieved by separating the surfaces by ~2 mm, inserting an ultraviolet

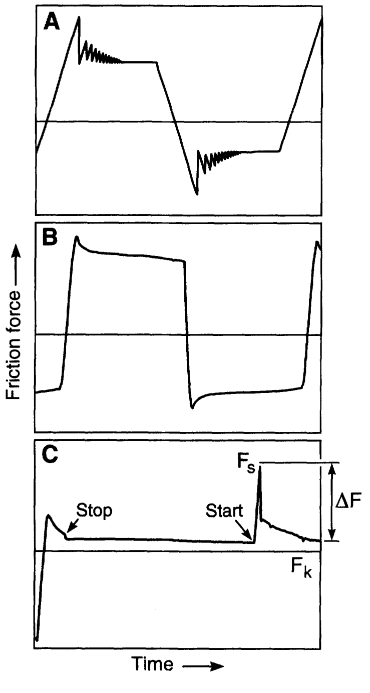

Fig. 2. Typical friction force profiles (friction traces) showing how *F* varies with the sliding time *t* for two symmetric polymer films. Qualitative features that are common to both polymers: (**A**) Decaying stick-slip motion observed until smooth sliding is attained if the motion continues for a sufficiently long distance (and even faster at higher sliding speeds). (**B**) Smooth sliding observed at sufficiently high speeds. (**C**) Stiction spike Δ*F* observed on recommencement of sliding after the surfaces have been kept at rest (in adhesive contact) for a given "stopping time" t_s.

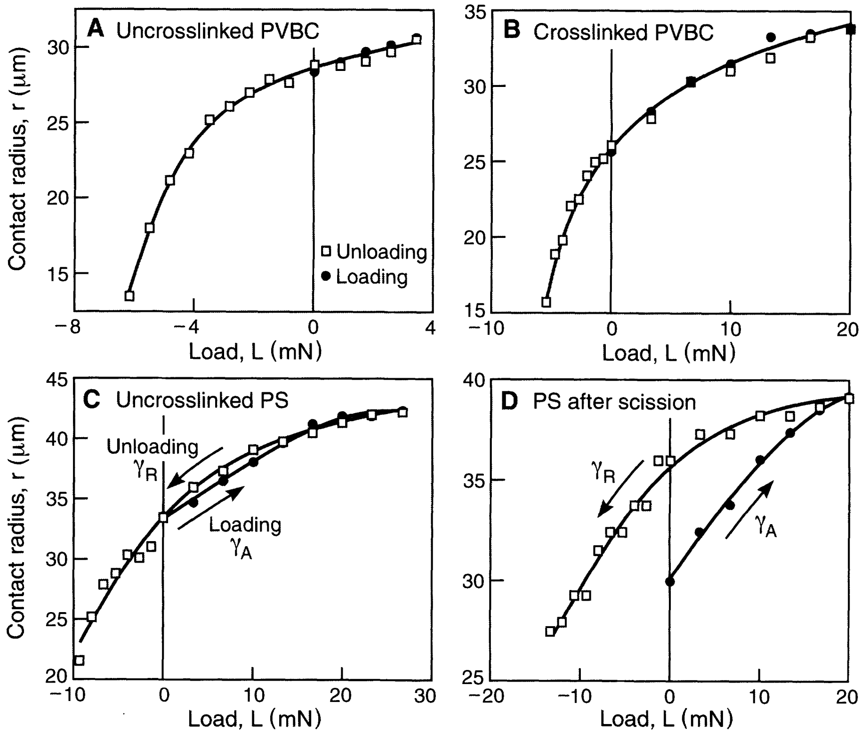

Fig. 3. Typical adhesion hysteresis or "JKR plots" of PS and PVBC surfaces in which the contact radius *r* (defined in Fig. 1) is plotted as a function of the externally applied load *L* (also defined in Fig. 1). According to the Johnson-Kendall-Roberts (JKR) theory (*8*, *25*), such plots should be reversible for elastic, nonhysteretic surfaces, and given by the so-called JKR equation (*8*, *25*). (**A**) Uncrosslinked PVBC surfaces. The size of the adhesion hysteresis is small. (**B**) Plot after crosslinking of PVBC surfaces. (**C**) Uncrosslinked PS surfaces. (**D**) Plot after chain scission of PS surfaces, after 18 hours of irradiation in an oxygen atmosphere. The adhesion hysteresis continues to increase with the UV irradiation time.

(UV) pen-ray lamp (Pen-Ray 90-0012-01; UVP Inc., Upland, CA), and irradiating the surfaces from a distance of about 1 cm in an atmosphere of dry nitrogen gas. The temperature rise at the surfaces during the UV irradiation was found to be small—a few degrees at most. The degree of crosslinking as a function of irradiation time was calibrated by the sol fraction method (*13*). We studied surfaces of different crosslinking density. For PVBC, once the fraction of crosslinked molecules exceeded 25% (averaged over the film), the tribological results did not change, indicating that the top layer was effectively fully crosslinked (*14*).

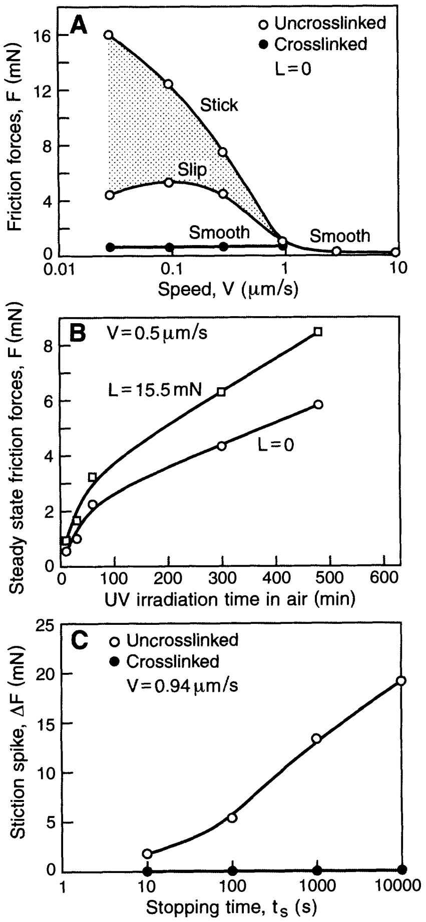

Fig. 4. Friction forces of PVBC and PS surfaces under various conditions. (**A**) Friction force F between two PVBC surfaces as a function of sliding speed V at zero applied load ($L = 0$) before and after crosslinking. At zero and low external loads, as shown here, the friction forces of the crosslinked and uncrosslinked surfaces fell to similarly low values at high V, for reasons discussed in the text. At higher loads (*16*) the uncrosslinked surfaces exhibited a higher friction at all sliding speeds. (**B**) The steady-state friction force of PS surfaces at a sliding speed of 0.5 μm/s and at two different loads as a function of UV irradiation time in air (i.e., containing oxygen gas). As chain scission proceeds, the friction force increases continually until it becomes too large ($F > 200$ mN) to be measured with the bimorph slider friction-detecting device used. (**C**) Stiction spikes ΔF between two PVBC surfaces as functions of stopping time t_s before and after crosslinking.

The friction forces of crosslinked PVBC surfaces were found to be a few orders of magnitude less than those of uncrosslinked surfaces, and no stick-slip motion was measured at any of the speeds studied (Fig. 4A). The reason for the large reduction in the friction force may be attributed to the inability of the crosslinked polymer segments at the interface to penetrate into the other surface (Fig. 1C). The similarity of the friction forces at high speeds in the two cases is likely to be the cause of this inability, due to the lack of time, of the uncrosslinked chains [mainly loops (*12*)] to penetrate the opposite surface at high V, which makes them behave like the crosslinked chains.

The corresponding adhesion hysteresis data (Fig. 3B) are not accurate enough to tell whether the (already small) hysteresis has diminished even further after cross-linking. It appears that a very small adhesion hysteresis that is beyond the limit of detection can still be accurately measured via friction measurements (*15*). Similar friction/adhesion results were obtained for PS (*14, 16*).

For PS, in situ chain scission is easily achieved by UV irradiation, but for a longer time and in the presence of oxygen gas (*17*). Chain scission involves the "chopping up" of the polymer chains, resulting in the exposure of "free" distal chain ends, but with restricted subsurface chain motion relative to the uncrosslinked polymer due to the attachment of their proximal ends. After scission of crosslinked PS, both the adhesion hysteresis (Fig. 3D) and friction forces (Fig. 4B) increased substantially. The friction forces could be raised to very high values, depending on the extent of the chain scission (UV irradiation time), until they became too large ($F > 200$ mN) to be measured with the bimorph slider friction-detecting device that was used (*18*). The marked rise in the friction and adhesion hysteresis of the scissed coils is attributed to exposure of "free ends" that are now able to penetrate deeply into the other surface (Fig. 1D), even though they are still attached to the surface at their proximal ends. As previously mentioned and illustrated in Fig. 1A, only a small amount of end-penetration is sufficient to produce very strong adhesion and friction. Furthermore, in high-MW polymers, the snake-like "reptational" motion of chain ends is very much more rapid than the translational motion of loops, coils, and hair-pin bends (*19*), which further enhances both of these effects. UV radiation in the presence of oxygen gas may also alter the surface chemistry by forming oxygen-containing groups, thereby increasing the polarity, which could also contribute to an enhanced friction. However, given the small difference in the adhesion hysteresis and friction between the nonpolar PS and polar PVBC surfaces, we believe that the major effect comes from chain scission.

"Stop-start" measurements were also made to establish the relaxation dynamics of the polymer chains at the shearing interfaces (*20*). In these, sliding is suddenly arrested while the surfaces are in smooth steady-state motion; the two surfaces are then kept in stationary contact for a given "stopping time" t_s before the sliding motion is resumed at the same velocity. If the stopping time is small, the surfaces usually continue to slide smoothly. Once the stopping time exceeds the time required for molecular rearrangements at the interface, an increasing resistance to motion, characterized by a stiction spike, occurs at the recommencement of sliding (Fig. 2C). Similar spikes may appear during sliding after each reversal of the sliding direction, because the surfaces are in stationary contact for a finite time during the reversal (Fig. 2, A and B). The height of the stiction spike $\Delta F = (F_s - F_k)$ as a function of the stopping time t_s gives a quantitative indication of the extent and dynamics of the molecular restructuring across the interface (*20, 21*). Figure 4C shows plots of ΔF versus t_s for two PVBC surfaces. Before crosslinking, the stiction spikes increase with the stopping time, reflecting the slow rearrangements of the "free" polymer chains—mainly loops (*12*)—across the interface. After crosslinking, the stiction spikes remain small and largely unchanged with time even for long stopping times, indicating that little rearrangement at the interface now occurs on the time scale of our experiments. After chain scission, the unmeasurably high stiction indicates very large restructuring (e.g., interpenetration) of the distally free ends across the interface.

We have studied what amounts to the friction at single asperity junctions having contact diameters of 10 to 100 μm, and there is every reason to believe that the results should apply to "real" engineering surfaces at the macroscale. The main difference is that extended rough surfaces have many contacting junctions (of similar magnitude to ours) where the net effect is a statistically averaged sum of the individual junctions. This averaging or summing is still an experimentally and theoretically challenging problem (*22*). Nevertheless, the trends observed here, such as the reduced adhesion hysteresis and friction of crosslinked compared to uncrosslinked polymer, are fully consistent with data on the (rolling) friction of rubber (*23, 24*).

For two shearing polymer surfaces, our results show that (i) the friction force is correlated with the adhesion hysteresis; (ii) both are determined mainly by the state of the polymer chains at or very near the surfaces; (iii) both can be manipulated by adjusting the degree of crosslinking and the density of free long chains and free ends at the surfaces (with freely protruding ends having the largest effect on adhesion hysteresis and friction as a result of their high local mobility); and (iv) a progressive rearrangement of the molecules and/or monomer segments at the shearing interface occurs during continuous sliding over large distances (many molecular dimensions)—that is, steady-state conditions do not occur instantaneously or even after a short shearing distance. Despite the apparent complexity of the adhesion and friction results, a fairly consistent and rational picture nevertheless emerges that can be understood in terms of the changing molecular configurations and motions of polymer chains and their segments at adhering and shearing junctions.

References and Notes

1. Y.-L. Chen, C. A. Helm, J. N. Israelachvili, *J. Phys. Chem.* **95**, 10736 (1991).
2. M. Heuberger, G. Luengo, J. Israelachvili, *J. Phys. Chem. B* **103**, 10127 (1999).
3. G. Luengo, M. Heuberger, J. Israelachvili, *J. Phys. Chem. B* **104**, 7944 (2000).
4. J. Israelachvili, A. Berman, *Origin of Energy Dissipation and Other Tribological Processes at the Molecular Level*, Proceedings of the International Tribology Conference III, 30 October to 2 November 1995, Yokohama, Japan (Japanese Society of Tribologists, 1996).
5. B. N. J. Persson, *Sliding Friction: Physical Principles and Applications* (Springer-Verlag, Berlin, 1998).
6. M. Tirrell, *Langmuir* **12**, 4548 (1996).
7. H. R. Brown, T. P. Russell, *Macromolecules* **29**, 798 (1996).
8. L. Li, V. S. Mangipudi, M. Tirrell, A. V. Pocius, in *Fundamentals of Tribology and Bridging the Gap Between the Macro- and Micro/Nanoscales*, B. Bhushan, Ed. (Kluwer Academic, Dordrecht, Netherlands, 2001), pp. 305–329.
9. G. Luengo, F.-J. Schmitt, R. Hill, J. Israelachvili, *Macromolecules* **30**, 2482 (1997).
10. J. N. Israelachvili, *J. Colloid Interface Sci.* **44**, 259 (1973).
11. We concentrate our discussion on the more significant changes observed. There is a tendency for the friction forces to increase with elevating temperature. There was also a slight increase in the friction forces for the thinner PS films: less than a factor of 2 difference for films whose thickness differed by an order of magnitude.
12. We use the term "loops" merely to distinguish these segments from "ends," of which there are only two per linear chain. Because of the high molecular weight of the polymers, most of the segments at the surface come from the interior parts of the chains, and are therefore in the form of "loops" regardless of whether or how much they protrude from the surface.
13. P. J. Flory, *Principles of Polymer Chemistry* (Cornell Univ. Press, Ithaca, NY, 1953).
14. The sol fraction data (*16*) and other considerations show that the crosslinking gradually proceeds from the top layer of the polymer film (the skin depth for UV light) into the bulk of the film. It is therefore reasonable to conclude that crosslinking of only the outermost layers of the polymer chains is sufficient to substantially reduce the friction.
15. This is because adhesion hysteresis is a measure of the difference between two values that are often close together, whereas friction forces have zero as the reference point.
16. N. Chen, N. Maeda, M. Tirrell, J. N. Israelachvili, in preparation.
17. C. S. Henkee, thesis, Cornell University (1985).
18. Once this occurs, the two surfaces remain stuck together even when the surface is sheared to its maximum amplitude (~130 μm in this case). The lower bound of the friction force (~0.2 N) is determined by the spring constant of the friction detection device.
19. G. Agrawal *et al.*, *J. Polym. Sci. Polym. Phys.* **34**, 2919 (1996).
20. H. Yoshizawa, Y.-L. Chen, J. Israelachvili, *J. Phys. Chem.* **97**, 4128 (1993).
21. A. D. Berman, J. N. Israelachvili, in *Modern Tribology Handbook*, B. Bhushan, Ed. (CRC Press, Boca Raton, FL, 2000), vol. 1, pp. 567–615.
22. B. N. J. Persson, *J. Chem. Phys.* **115**, 5597 (2001).
23. A. D. Roberts, A. G. Thomas, *Wear* **33**, 45 (1975).
24. A. D. Roberts, *Rubber Chem. Technol.* **52**, 23 (1979).

→ K. L. Johnson, K. Kendall, A. D. Roberts, *Proc. R. Soc. London Ser. A* **324**, 301 (1971).

26. We thank E. Kramer and J. Benkoski for helpful discussions, G. Carver for technical assistance, and D. McLaren for the artwork. Supported by U.S. Department of Energy grant DE-FG03-87ER 45331 (J.N.I., N.C., and N.M.).

29 March 2002; accepted 10 May 2002

Rapid Wastage of Alaska Glaciers and Their Contribution to Rising Sea Level

Anthony A. Arendt,* Keith A. Echelmeyer, William D. Harrison, Craig S. Lingle, Virginia B. Valentine

We have used airborne laser altimetry to estimate volume changes of 67 glaciers in Alaska from the mid-1950s to the mid-1990s. The average rate of thickness change of these glaciers was −0.52 m/year. Extrapolation to all glaciers in Alaska yields an estimated total annual volume change of −52 ± 15 km^3/year (water equivalent), equivalent to a rise in sea level (SLE) of 0.14 ± 0.04 mm/year. Repeat measurements of 28 glaciers from the mid-1990s to 2000–2001 suggest an increased average rate of thinning, −1.8 m/year. This leads to an extrapolated annual volume loss from Alaska glaciers equal to −96 ± 35 km^3/year, or 0.27 ± 0.10 mm/year SLE, during the past decade. These recent losses are nearly double the estimated annual loss from the entire Greenland Ice Sheet during the same time period and are much higher than previously published loss estimates for Alaska glaciers. They form the largest glaciological contribution to rising sea level yet measured.

Mountain glaciers (*1*) constitute only about 3% of the glacierized area on Earth, but they are important because they may be melting rapidly under present climatic conditions and may therefore make large contributions to rising sea level. Previous studies (*2*–*7*), based on observations and model simulations of glacier mass balance, estimated the contribution of all mountain glaciers to rising sea level during the last century to be 0.2 to 0.4 mm/year. The range of uncertainty is large, and it stems from insufficient measurements of glacier mass balance: Conventional mass balance programs are too costly and difficult to sample adequately the >160,000 glaciers on Earth. At present, there are only about 40 glaciers worldwide with continuous balance measurements spanning more than 20 years (*8*). High-latitude glaciers, which are particularly important because predicted climate warming may be greatest there (*7*), receive even less attention because of their remote locations. Glaciers that are monitored routinely are often chosen more for their ease of access and manageable size than for how well they represent a given region or how large a contribution they might make to changing sea level. As a result, global mass balance data are biased toward small glaciers (<20 km^2) rather than those that contain the most ice (>100 km^2). Also, large cumulative errors can result from using only a few point measurements to estimate glacier-wide mass balances on an individual glacier.

Glaciers in Alaska and neighboring Canada (labeled "Alaska" glaciers herein) cover 90,000 km^2 (*9*), or about 13% of the mountain glacier area on Earth (*10*), and include some of the largest ice masses outside of Greenland and Antarctica. Additionally, many of these glaciers have high rates of mass turnover. However, they are underrepresented by conventional mass balance studies, which include only three or four long-term programs on relatively small glaciers. Dyurgerov and Meier (*5*), by necessity, extrapolated the data from these few small glaciers to estimate the contribution of all Alaska glaciers to sea-level change, and they specifically pointed to the need for further data in this region, especially on the larger glaciers. Here, we use airborne laser altimetry to address this problem. We have measured volume and area changes on 67 glaciers, representing about 20% of the glacierized area in Alaska and neighboring Canada, and we use these data to develop new estimates of the total contribution of Alaska glaciers to rising sea level.

Our altimetry system consists of a nadir-pointing laser rangefinder mounted in a small aircraft and a gyro to measure the orientation of

---

Geophysical Institute, University of Alaska, 903 Koyukuk Drive, Post Office Box 757320, Fairbanks, AK 99775, USA.

To whom correspondence should be addressed: E-mail: arendta@gi.alaska.edu